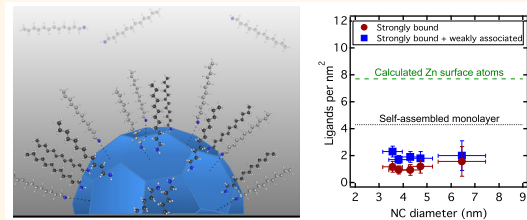


Low Capping Group Surface Density on Zinc Oxide Nanocrystals

Carolyn N. Valdez,[†] Alina M. Schimpf,[†] Daniel R. Gamelin,[†] and James M. Mayer^{†,‡,*}

[†]Department of Chemistry, University of Washington, Seattle, Washington 98195-1700, United States and [‡]Department of Chemistry, Yale University, New Haven, Connecticut 06520, United States

ABSTRACT The ligand shell of colloidal nanocrystals can dramatically affect their stability and reaction chemistry. We present a methodology to quantify the dodecylamine (DDA) capping shell of colloidal zinc oxide nanocrystals in a nonpolar solvent. Using NMR spectroscopy, three different binding regimes are observed: strongly bound, weakly associated, and free in solution. The surface density of bound DDA is constant over a range of nanocrystal sizes, and is low compared to both predictions of the number of surface cations and maximum coverages of self-assembled monolayers. The density of strongly bound DDA ligands on the as-prepared ZnO NCs is 25% of the most conservative estimate of the maximum surface DDA density. Thus, these NCs do not resemble the common picture of a densely capped surface ligand layer. Annealing the ZnO NCs in molten DDA for 12 h at 160 °C, which is thought to remove surface hydroxide groups, resulted in a decrease of the weakly associated DDA and an increase in the density of strongly bound DDA, to *ca.* 80% of the estimated density of a self-assembled monolayer on a flat ZnO surface. These findings suggest that as-prepared nanocrystal surfaces contain hydroxide groups (protons on the ZnO surfaces) that inhibit strong binding of DDA.



KEYWORDS: capping ligands · colloidal semiconductors · zinc oxide · ligand shell · NMR spectroscopy of nanocrystals

Colloidal semiconductor nanocrystals (NCs) are widely investigated for use in solar cells, light emitting devices, luminescent biological labels, and many other applications.^{1–3} NCs are unique materials, combining the tunable electronic structure and photochemical properties associated with bulk materials with the synthetic accessibility and spectroscopic convenience of small molecules.^{4,5} Most NC preparations in nonpolar solvents use capping ligands to control solubility, photoluminescence, and other properties.^{6,7} The capping ligand density of each system is an important parameter to a range of chemical and physical properties of NCs, such as the inner sphere reactivity of NCs with hole acceptors⁸ and proton-coupled electron transfer (PCET) acceptors,^{9,10} as well as interparticle electron transfer.¹¹

Recent studies show that the capping ligands on semiconductor NCs are more complex and dynamic than the traditional image of a fairly dense shell.^{8–17} In work related to that reported here, Kahn *et al.* identified different types of dodecylamine (DDA) in the ligand shells of large ZnO NCs (prepared by a different synthetic method),¹⁵ but they did not quantify the number of

capping ligands per NC. The literature of capping groups on other semiconductor NCs, especially CdSe, is much more extensive.^{13,16,18–20} In particular, Weiss *et al.* have reported that the density and dynamics of the capping groups strongly influence the chemical reactivity of chalcogenide NCs.⁸

Of the variety of techniques that have been used to examine the chemistry of capping ligands,^{16,21} NMR spectroscopy is especially powerful. NMR spectroscopy is an *in situ* and nondestructive analysis that provides information about the organic molecules interacting with NCs in solution.¹³ The *in situ* nature of NMR spectroscopy is particularly valuable for examining the capping ligands under conditions that parallel reactivity and spectroscopic studies. Diffusion-ordered NMR spectroscopy (DOSY) and related exchange spectroscopies have been used to investigate the interaction of ligands with NC surfaces^{15,22} and to extract overall sizes using the Stokes–Einstein relation.^{15,23}

Here, we report analyses of the DDA ligand shell in a series of ZnO NC samples suspended in toluene. A method to quantify capping group densities on ZnO NCs is described. NMR spectroscopic data

* Address correspondence to
james.mayer@yale.edu.

Received for review July 2, 2014
and accepted August 17, 2014.

Published online August 18, 2014
10.1021/nn503603e

© 2014 American Chemical Society

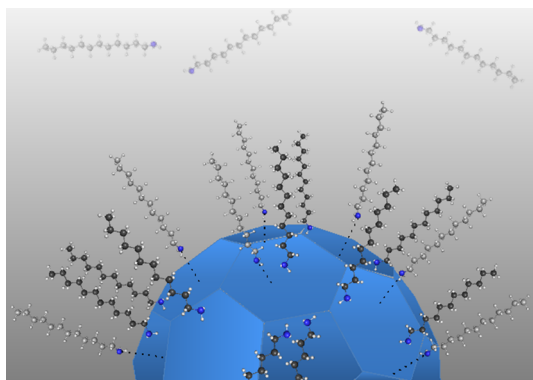


Figure 1. Illustration of one quadrant of a faceted NC ($d = 3.8$ nm) with DDA capping ligands. The proportion of strongly bound (black carbon atoms) and weakly bound DDA (gray carbon atoms) is depicted in the proportions measured by NMR spectroscopies, showing the sparse surface coverage by DDA.

implicate a model with strongly bound, weakly associated, and free DDA. The strongly bound DDA ligands cover only 10–20% of the estimated number of surface Zn atoms and account for less than 25% of the maximum coverage predicted for a self-assembled monolayer. Figure 1 is a quantitative illustration of the measured density, roughly to scale. It shows a quarter of a 3.8 nm NC with its roughly 10 strongly bound DDA ligands and slightly fewer weakly bound DDA groups. Thus, these NCs have very incomplete surface shells of capping ligands, which contrasts with the typical view. Annealing the NCs causes an increase in the coverage of the strongly bound ligands and a decrease of weakly associated ligands. Since annealing causes the loss of water, this result supports the hypothesis that strong binding of DDA is blocked by surface protons (hydroxide ligands).

RESULTS AND DISCUSSION

Characterization of Dodecylamine Bound to ZnO Nanocrystals

ZnO NCs with average diameters (d) between 3 and 7 nm were synthesized at room temperature in multi-gram batches by the wet chemical method described previously,²⁴ capped with DDA, suspended in toluene and stored at -35 °C. The mean ZnO NC size was determined from the position of the first exciton peak^{25,26} or by transmission electron microscopy (TEM). The total Zn concentration in the solution was measured by inductively coupled plasma-optical emission spectrometry (ICP-OES).¹⁷ These data give the concentration of NCs, which was on the order of 0.01–1 mM for the experiments described here. Figure 2 compares a typical ^1H NMR spectrum of capped ZnO NCs in toluene- d_8 versus DDA alone. For ZnO and similar systems, ^1H NMR resonances of ligands in the presence of NCs often appear downfield of the free ligand and are significantly broadened.^{22,27} Broadening of the NMR ligand signals likely arises from multiple effects, including slow tumbling of the large NCs, decreased T_2 ,

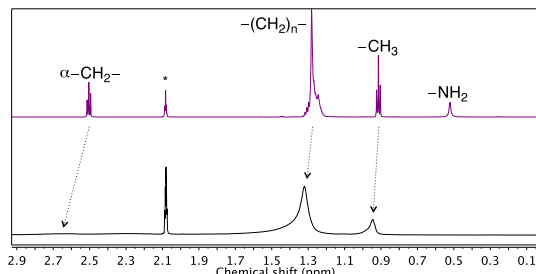


Figure 2. ^1H NMR spectra (700 MHz) of DDA only (top) and capped ZnO NCs (bottom) in toluene- d_8 , NC $d = 4.3$ nm, $[\text{NCs}] = 6 \times 10^{-4}$ M, and the asterisk refers to the residual solvent signal. In the presence of NCs, the $\alpha\text{-CH}_2$ signal is broadened and the amine peak is not observed.

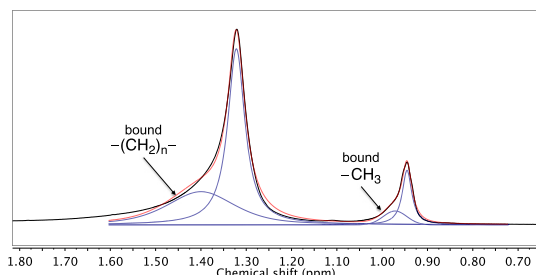


Figure 3. Fitting of the aliphatic signals in the ^1H NMR spectrum of ZnO/DDA solutions (the same data as in Figure 2). The experimental spectrum is shown in black, the blue traces are individual peak fits, and the red is the sum of the fits.

heterogeneity of the NCs in size, shape and surface properties, and the relatively high viscosity of the solutions.¹³ In the presence of ZnO NCs, the signal at 0.4 ppm for the DDA NH_2 group disappears, the $\alpha\text{-CH}_2$ peak is broadened and shifted downfield (to ~ 2.7 ppm), and the methyl and composite methylene peaks ($-\text{CH}_3$, 0.9 ppm; $-(\text{CH}_2)_{10}-$, 1.3 ppm) broaden and develop downfield shoulders (Figure 2).

The ^1H NMR resonance for the internal methylene protons ($-(\text{CH}_2)_{10}-$) in ZnO/DDA solutions is well modeled as the sum of two peaks: one broad and more downfield (1.37 ppm), the other sharper and slightly upfield (1.31 ppm) (Figure 3). The $-\text{CH}_3$ resonances are also well modeled as two peaks, and essentially the same ratio of broad to sharper peaks is obtained. On the basis of the peak positions and widths, and the DOSY experiments described in detail below, the broad downfield signals are assigned to DDA strongly bound to the NCs. With larger NCs, the distinction between the broad and sharp signals is even more pronounced.

DOSY and Nuclear Overhauser Effect spectroscopy (NOESY, see Supporting Information) confirmed that the broad downfield peaks correspond to DDA bound to the NCs. A ^1H DOSY NMR spectrum of the ZnO NCs in toluene- d_8 is shown in Figure 4. DOSY is a pseudo-two-dimensional technique, displayed with the one-dimensional ^1H NMR spectrum on the horizontal axis and diffusion coefficient (D) along the vertical axis.

D can be related to the hydrodynamic radius R_H via the Stokes–Einstein relation eq 1, where k_B is the Boltzmann constant, T is the absolute temperature, and η is the viscosity of the solution.^{15,16} D is inversely proportional to R_H because larger species move more slowly in solution. Trimethoxybenzene (TMB) was added to the solution as an internal standard, and analysis of its resonances at 3.3 and 6.1 ppm gave a diffusion constant of $1.6 \times 10^{-9} \text{ m}^2 \text{ s}^{-1}$, which is typical for a small molecule.²³

$$D = \frac{k_B T}{6\pi\eta R_H} \quad (1)$$

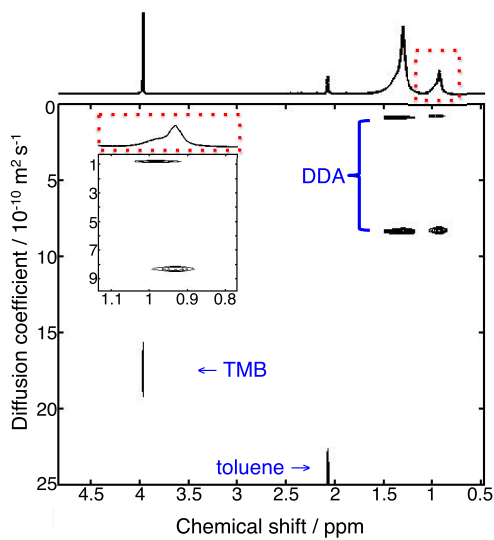


Figure 4. Typical ^1H DOSY NMR spectrum of ZnO NCs with DDA capping ligands in toluene- d_8 . The data processing was done with DOSYToolbox 1.5, using Local Covariance Order Diffusion-Ordered Spectroscopy (LOCODOSY) for better resolution of the overlapping peaks.²⁸ Inset shows just the DDA methyl peak (dotted red box) to highlight the differences in chemical shift between the strongly bound DDA and the faster diffusing DDA.

In the DOSY spectrum, the DDA signals between 0.5 and 2 ppm are split into two separate diffusion regimes (Figure 4, top). The D for the more slowly diffusing DDA peaks, $1.1(4) \times 10^{-10} \text{ m}^2 \text{ s}^{-1}$ (errors reported in parentheses are twice the standard deviation from replicates), corresponds to the broad down-field resonance shown in Figure 3. This D implies a hydrodynamic radius of 7 nm by eq 1. This was confirmed in separate experiments by referencing to the D of ferrocene in the same solution ($R_H(\text{Cp}_2\text{Fe}) = 0.3 \text{ nm}$ ²³). The diameters obtained by the DOSY experiments are roughly the NC diameter size plus two ligands (see Supporting Information), which suggests that the NCs are not significantly aggregated. The assignment of these slowly diffusing DDA molecules as strongly bound is consistent with literature precedent,¹⁵ and is supported by a dilution experiment. Dilution of a sample of colloidal NCs by a factor of 5 led to no change in the strongly bound DDA groups per NC (*vide infra*). The diffusion peaks at $\sim 1 \times 10^{-10} \text{ m}^2 \text{ s}^{-1}$ are thus assigned as strongly bound ligands, and this value is termed D_{bound} . This apparent diffusion constant did not vary between batches of NCs that contain varying amounts of free DDA. These results indicate that strongly bound DDA do not exchange with free DDA on the NMR time scale (Table 1).

In contrast, the D values for the faster diffusing DDA peaks vary considerably from batch to batch, between 4.9 and $9.7 \times 10^{-10} \text{ m}^2 \text{ s}^{-1}$. To study this variability, extra DDA (65 per NC) was added to a solution of as-prepared NCs, and a new DOSY NMR spectrum was recorded (Table 1, NC batch B*). With excess DDA, the diffusion peak shifted to larger D values. This observation indicates that the second diffusion peak corresponds to species in a rapid equilibrium with free DDA, resulting in an averaged diffusion coefficient. This result implies that this diffusion constant corresponds

TABLE 1. Quantification of Dodecylamine Ligands on a Variety ZnO NCs Batches Using ^1H and DOSY NMR Data

NC batch	NC diameter ^a	D_{bound}^b	D_{mix}^c	χ_{bound}^d	χ_{weak}^e	χ_{free}^e	surface area (nm^2) ^f	total DDA/NC	DDA bound/NC	DDA weak/NC	DDA free/NC	ligand/ nm^2 (bound + weak)	ligand/ nm^2 (bound)
A	3.6(4)	0.9(1)	7.1(1.4)	0.43(6)	0.32(12)	0.26(10)	40	120(40)	50(20)	40(10)	30(10)	2.1(2)	1.2(2)
B	3.8(4)	0.9(2)	4.9(9)	0.47(5)	0.38(8)	0.15(8)	46	100(30)	40(15)	35(10)	25(15)	1.7(4)	0.9(3)
B* ^g	3.8(4)	0.9(2)	9.3(14)	0.39(15)	0.23(2)	0.39(16)	46	140(40)	50(20)	30(10)	60(20)	1.8(3)	1.1(4)
B** ^g	3.8(4)	0.9(1)	5.9(6)	0.47(5)	0.34(3)	0.20(2)	46	90(20)	40(15)	30(10)	20(5)	1.6(4)	0.9(3)
C	4.3(4)	1.3(3)	6.8(4)	0.34(6)	0.39(4)	0.27(2)	58	150(30)	55(10)	55(15)	40(10)	1.9(4)	0.9(2)
D	4.7(5)	1.1(4)	9.7(13)	0.39(4)	0.22(10)	0.40(14)	70	220(80)	85(40)	45(10)	90(40)	2.0(5)	1.2(4)
E	6.5(20)	0.9(1)	9.0(12)	0.59(4)	0.17(8)	0.24(6)	131	340(190)	200(100)	60(40)	70(50)	2.0(11)	1.6(8)
F _{annealed}	9.2(10)	1.1(10)	12(1)	0.51(8)	0.10(4)	0.39(6)	266	1870(100)	920(80)	200(100)	760(30)	4.2(3)	3.4(2)
G _{annealed}	9.5(10)	0.8(2)	7.1(14)	0.89(12)	0.06(4)	0.05(3)	284	1180(120)	1030(100)	90(70)	60(40)	4.0(2)	3.6(2)

^a Average diameter of the NCs in the batch (values in nm), from the position of the first exciton peak (for $d < 7 \text{ nm}$)²⁵ or TEM (for larger NCs), and the error is reported in parentheses as 10% or the standard deviation derived from TEM, respectively. ^b D values in units of $10^{-10} \text{ m}^2/\text{s}$ and data are averaged using at least two of each 1D ^1H and DOSY experiments. Errors are calculated as two standard deviations from replicates or 10%, whichever was greater. ^c D_{mix} is the averaged diffusion coefficient between weakly bound and free DDA. ^d The mole fraction of strongly bound DDA (χ_{bound}) was calculated from fitting of a 1D NMR spectrum. ^e The mole fractions were calculated using eqs 2 and 3, assuming there are only three different classes of DDA in these solutions with ZnO NCs. $D_{\text{free}} = 1.45 \times 10^{-9} \text{ m}^2/\text{s}$ for all of the calculations. ^f Diameter and surface area of the ZnO NCs without capping ligands, calculated assuming a spherical shape. ^g Batch labeled B* corresponds to batch B plus 65 equiv of DDA per NC. Batch labeled B** corresponds to batch B diluted a factor of 6 to a final concentration of $1.3 \times 10^{-4} \text{ M}$ in NCs.

to more than one “type” of DDA, with one of the species interacting with the NCs.²⁹ Therefore, this peak is termed D_{mix} , the diffusion peak corresponding to the concentration-dependent equilibrium between free DDA and weakly associated DDA.

Here “weakly associated” encompasses all of the bound DDA molecules that exchange rapidly with free DDA and are not strongly bound to the NC surface like those with D_{bound} . The nature of the bonding of the weakly associated DDA could involve Zn^{2+} sites that are less Lewis-acidic, van der Waals interactions of the hydrocarbon chains with the strongly bound DDA (perhaps with the amine pointing out), and/or hydrogen bonding between the amine and the NC surface. Experiments with annealed nanocrystals discussed below favor a hydrogen bonding interaction with surface hydroxide groups.

The NMR data are well modeled using these three different classes of DDA binding to NCs: free, weakly associated, and strongly bound. A similar distinction between different levels of DDA association was presented in the study by Kahn *et al.*¹⁵ They measured approximate rate constants of $k_{\text{off-strong}} = 13 \text{ s}^{-1}$ for dissociation of strongly associated DDA and $k_{\text{off-weak}} = 25 \times 10^5 \text{ s}^{-1}$ for dissociation of weakly associated amines.¹⁵ This fast desorption rate of weakly associated amine from the NC surface is consistent with the rapid exchange with free DDA in the NMR spectra reported here.

Quantification of the Number of Dodecylamine Ligands in Each Regime. One benefit of the averaged D_{mix} in this two-state model is the ability to determine the molar fractions of free and weakly associated DDA. For example, in a system with 100% free DDA (i.e., no weakly associated), D_{mix} would be equal to D_{free} . The two unknown mole fractions χ_{weak} and χ_{free} are determined from the set of two equations below, using the fraction of strongly bound DDA (χ_{bound}) calculated from integration of a 1D ^1H NMR spectrum (Figure 3), and assuming that the unknown D_{weak} is equal to D_{bound} .²²

$$D_{\text{mix}} = \chi_{\text{weak}} D_{\text{weak}} + \chi_{\text{free}} D_{\text{free}} \quad (2)$$

$$\chi_{\text{free}} + \chi_{\text{weak}} + \chi_{\text{bound}} = 1 \quad (3)$$

Combining the data allows the calculation of the absolute number of bound DDA molecules per NC. The mole fractions and the NMR integrations versus an internal standard give the concentration of each class of DDA. The concentration of NCs is given by the total Zn concentration (from ICP-OES) divided by the average number of Zn per NC.¹¹ Remarkably, 3.8 nm ZnO NCs have only 40–50 strongly bound DDA ligands.

The number of capping groups per squared nanometer (nm^2) of NC surface area, also known as the ligand density, is given in Table 1. These calculations assume a spherical shape for the ZnO NCs. The average

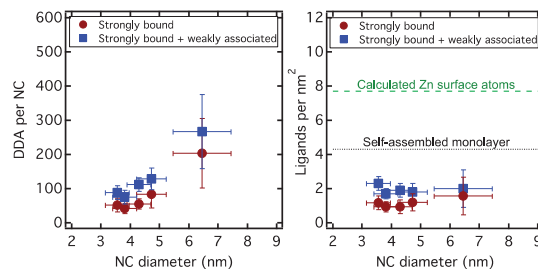


Figure 5. Number of DDA per NC versus NC diameter (left), and the number of ligands per nm^2 versus NC diameter (right). Errors are calculated as two standard deviations from replicates or 10%, whichever was greater. Black dotted line indicates SAM coverage for single crystal ZnO ($4.2/\text{nm}^2$),³⁰ and green dashed line indicates the coverage predicted with one DDA per calculated surface Zn ($\sim 7.7/\text{nm}^2$, average calculated from Table 2).

ligand densities are remarkably constant across all as-prepared batches of NCs and sizes (Figure 5). The average ligand density of strongly bound DDA only is $1.0(3)/\text{nm}^2$, and the density of both strongly bound and weakly associated DDA is $1.9(4)/\text{nm}^2$. Different values are found for annealed NCs, as discussed below.

Comparison of Ligand Surface Density to Surface Cation Estimates or SAMs. The significance of the observed surface ligand densities is revealed by comparison with the maximum surface coverage. To assess the maximum surface coverage, one can (1) estimate the number of available surface Zn binding sites or (2) compare to maximum coverage of similar ligands in the self-assembled monolayer (SAM) literature. There are a number of published methods to estimate the number of surface ions. The values given in Table 2 use the method of Kuno *et al.*¹⁹ that counts any Zn atom within 2.0 Å of the surface (one Zn–O bond length³¹). The many other published methods all give higher numbers of surface Zn ions (as discussed in the Supporting Information), so the values in Table 2 are lower estimates of surface Zn per NC. Including both the weakly associated and strongly bound ligands, the surface Zn sites are 25(6)% covered, independent of NC size and concentration. Considering only strongly bound DDA ligands gives 15(5)% coverage of surface Zn. Thus, a quarter or less of the calculated Zn surface atoms are bound to DDA according to surface cation calculations.

It is also informative to compare capping densities to maximum coverages achieved in SAMs. In this literature, the maximum coverage or saturation is often defined as “the highest possible packing of molecules”, which generally does not correspond to one ligand per surface Zn atom.³² For single crystal ZnO(1010) surfaces, Chen *et al.* found that although DDA did not form a stable monolayer, similarly sized or larger thiols and phosphonic acids formed monolayers with surface coverages of 4.2 and 4.4 molecules per nm^2 , respectively.³⁰ In the gold nanoparticle literature, Hinterwirth *et al.* observed higher ligand densities on nanoparticles than

TABLE 2. Calculation of Surface Coverage Using the Number of Zn Unit Cells per NC^a

NC batch	NC diameter (nm)	surface Zn atoms ^a	% surface Zn with strong + weak DDA	% surface Zn with strong DDA	Zn surface atoms without DDA ^b
A	3.6(4)	300	30%	18%	210(30)
B	3.8(4)	340	22%	12%	270(30)
C	4.3(4)	440	25%	12%	330(20)
D	4.7(5)	540	24%	15%	410(60)
E	6.5(20)	1030	26%	20%	760(100)
F _{annealed}	9.2(10)	2140	58%	48%	900(200)
G _{annealed}	9.5(10)	2280	49%	45%	1160(50)

^aCalculated assuming that all Zn atoms within 2 Å of the surface (one Zn—O bond) can be considered a surface Zn, following Kuno *et al.*¹⁹ ^bThis estimate is conservative because it assumes both strongly bound and weakly associated DDA occupy Zn sites, and assumes fewer surface atoms than most estimates in the literature (see Supporting Information).

on a flat surface, up to 6.3 per nm², *versus* the theoretical 4.6 per nm² maximum coverage for a flat surface.³² These authors suggest the higher coverage arises from the existence of edges and corners in a spherical nanoparticle. Thus, taking the nonpolar ZnO(10̄10) surface as representative of the various nanocrystal surfaces, the small DDA capping group should provide a maximum surface coverage of >4.2 per nm² on ZnO, and likely higher due to the small footprint of DDA and the edges and corners inherent to a quasi-spherical NC. Considering strongly bound DDA ligands only, the ligand density of ZnO NCs reported here, 1.0(3) per nm², is less than 25(8)% of the 4.2 per nm² lower estimate anticipated for a ZnO SAM. If the weakly associated DDA molecules are also counted, the total ligand density of 1.9(4) per nm² rises to only 45(10)% of that anticipated for a SAM.

Reported surface densities for *anionic* ligands such as oleate and TOPO-derived anions, on chalcogenide and phosphide NCs, span values from 0.57 to 5 per nm².^{13,33–37} These have been determined using ¹H NMR spectroscopy, thermogravimetric analysis (TGA), or X-ray photoelectron spectroscopy (XPS). It is important to distinguish neutral (“L-type”) capping ligands, like DDA, from anionic ligands such as carboxylates or phosphonates (“X-type”). Dissociation of X-type ligands typically require stoichiometric protons, forming HX, and the activity and concentration of these protons may be a key factor for ligand coverage.³⁸ Comparisons between ZnO and chalcogenide NCs are complicated not only by the different ligand types but also by different unit cell sizes (unit cell volumes: CdSe, 112.2 Å³; ZnO, 47.6 Å³),³⁹ which imply different cation surface densities.

In sum, the surface coverages of as-prepared ZnO nanocrystals by strongly bound and weakly associated DDA are quite low compared to the typical image of a fully covered NC, by comparison to both surface cation estimates and the maximum coverage estimated for SAMs.

Origin of Low Capping Group Coverage. The low surface coverage could have a number of origins: sterics, inaccessibility of Zn sites, or blockage by other species. We discuss each of these possibilities in turn.

The density of capping ligands on NCs has been examined theoretically, as in Bullen and Mulvaney's modeling of a spherical NC with ligands represented by cones.⁴⁰ They estimated maximum surface coverage for large ligands such as trioctylphosphine oxide (TOPO) to be limited by steric bulk to only 30% of Cd + Se surface atoms for a 3.4 nm NC. Katari *et al.* found these estimates to agree with experimental X-ray photoelectron spectroscopy (XPS) coverage estimates of TOPO on CdSe.²⁰ However, terminal, linear aliphatic amines such as DDA have a much smaller “swept-out” cone radius,⁴⁰ which should allow binding to all surface metal atoms even on a flat surface (see Supporting Information). X-ray structures of small-molecule μ -oxo bridged Zn clusters with amine ligands also suggest that sterics should not limit DDA binding density.⁴¹ Therefore, sterics are unlikely to play a part in the low surface coverage.

The low observed DDA coverage may also be caused by blockage of Zn sites by other surface species or “ligands” for Zn. The likely candidates are DMSO, hydroxide, or ethoxide, since the NCs are formed in a hydrolytic process that involves ethanol and DMSO.²⁴ Unfortunately, such surface species are not directly observable by ¹H NMR spectroscopy. Alcohols are known to dissociate on the polar ZnO(0001) face to form stable alkoxide intermediates.⁴² In support of this hypothesis, added ethanol does reversibly interact with the NCs as judged by a change in the ¹H NMR chemical shift of the added EtOH. Treating NCs with ethanol-d₆ produced some CH₃CH₂OD, by ¹H NMR spectroscopy, but only a very small amount, <10 per NC (see Supporting Information). Thus, there is a small concentration of exchangeable ethanol/ethoxide on the surface, but not enough to account for the low DDA coverage observed here. Similarly, DMSO has not been observed in any of the NMR spectra. Some have suggested that “residual water” is associated with ZnO and CdTe,^{15,22} but released water was not observed in the NMR spectra for the samples described here. Annealing to remove associated water/hydroxide is discussed below.

Another possible origin of the low DDA coverage is that the exposed NC surfaces are oxide rich. Of the four

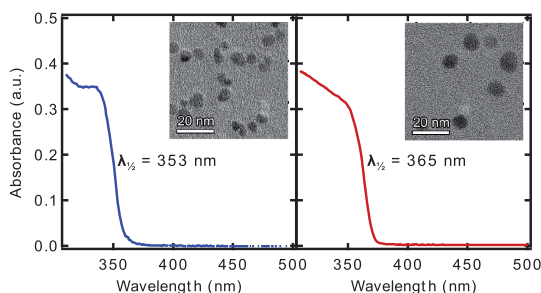


Figure 6. Optical absorption spectra in toluene and TEM images (insets) of batches B ZnO NCs (left, $d = 3.8(4)$ nm) and annealed F_{annealed} (right, $d = 9.2(10)$ nm). We note that sample B had aged for several months before the TEM analysis, and the particles grew slightly, so a more accurate determination of the size was accomplished using $\lambda_{1/2}$ according to ref 25.

most common surfaces of wurtzite ZnO, $(10\bar{1}0)$ and $(11\bar{2}0)$ are nonpolar and therefore balanced in Zn and O atoms, (0001) is primarily Zn terminated and $(000\bar{1})$ is primarily O-terminated.^{43,44} However, TEM images of the as-prepared NCs show very little faceting and are likely mixed surfaces. Annealing is suggested to increase the fraction of the low energy $(10\bar{1}0)$ surfaces,¹⁷ but little to no faceting is observed in the TEM images of our annealed samples (*vide infra*). Overall, the spherical nature of the NCs and the lack of faceting in the TEM images suggest that surface faceting is unlikely the origin of the low coverage of strongly bound DDA.

It is most likely that the low DDA coverage is due to the presence of surface hydroxide ligands, which reduces the number of sites available for DDA binding. Indeed, ZnO NCs prepared by this method show OH stretches in their IR spectra. Heating in molten DDA causes these OH stretches to disappear, suggesting loss of H_2O .¹⁷ The hypothesis that surface hydroxide ligands block DDA binding was tested by performing a similar annealing experiment, in which the present ZnO NCs were heated in molten DDA at $160\text{ }^{\circ}\text{C}$ for 12 h. TEM images show that the initial NCs ($d = 3.8(4)$ nm) grow upon annealing, in this case to $d = 9.2(10)$ nm (Figure 6). Efforts to make annealed NCs of the same size as room temperature as-prepared NCs ($d < 7$ nm) were unsuccessful, as observed in previous reports of DDA annealed NCs.¹⁷ Previous studies have indicated that the annealed NCs are more predominantly hexagonal and therefore likely enriched in the lowest energy ZnO $(10\bar{1}0)$ surfaces,^{17,44} although such hexagonal faceting is not evident in our images. ^1H and DOSY NMR analysis was performed to quantify the number of DDA ligands on the surface. The annealed NCs showed dramatic changes in the associated DDA, with a decrease in the density of weakly bound ligands and an increase in strongly bound ligands. The density of strongly bound DDA increases by a factor of 3 or more, to $3.5(3)$ per nm^2 . This corresponds to ca. 45% of the estimated surface Zn atoms covered with strongly bound DDA, and is

~80% of the estimated coverage for a SAM on single crystal ZnO.

Annealing reduces the number of weakly associated ligands to $0.6(3)$ nm^{-2} , reduces the number of surface hydroxides,¹⁷ and increases the number of strongly bound DDA molecules. One comprehensive explanation for these observations is that surface hydroxides can be considered “ligands” for Zn atoms at the surface, thereby blocking those cations from DDA. As annealing removes the hydroxides, the Zn sites are now open for a strong bond between Zn and the N of DDA. The robust binding is surprising because neutral monodentate alkylamines are not particularly strong ligands for Zn^{2+} in molecular coordination chemistry.^{45,46} A roughly equivalent description is that the NCs are proton-terminated ZnO, and the strongly bound DDA binds to Zn atoms exposed by surface oxygen vacancies. Annealing with loss of H_2O forms more surface oxygen vacancies and therefore strongly binds more DDA.

The weakly associated DDA ligands likely form hydrogen bonds to the hydroxides in the nonannealed NCs. This is more likely than purely van der Waals forces between the long aliphatic chains because of the decrease of the weakly associated DDA upon removal of hydroxide.

CONCLUSIONS

The surface coverage of neutral DDA capping ligands on ZnO NCs suspended in toluene solvent is investigated using a variety of NMR spectroscopies. Rather than a picture of a densely packed shell of ligands, our results implicate sparse or patchy coverage of amine capping ligands. 1D and DOSY ^1H NMR spectroscopies indicate that the DDA molecules in NC solutions can be divided into three categories: strongly bound, weakly associated, and free DDA. There are only *ca.* 15(5)% strongly bound DDA ligands per estimated surface zinc atom, which is less than 25(8)% of the coverage for a self-assembled monolayer. Figure 1 above is a fairly dramatic illustration of the low density found. NCs annealed at $160\text{ }^{\circ}\text{C}$ for 12 h in molten DDA, which are thought to have fewer surface hydroxyl groups,¹⁷ have more than three times the surface coverage of strongly bound DDA (1.0(3) to $3.5(3)$ per nm^2 , respectively). This suggests that annealing causes the replacement of surface hydroxide ligands by DDA. Equivalently, the NCs could be described as proton-terminated ZnO, and annealing causes loss of H_2O to form surface oxygen vacancies, bare Zn atoms, that strongly bind DDA.

The as-synthesized NCs have a substantial amount of weakly associated DDA, from 30 to 100% of the strongly bound ligands. These DDA ligands are much less abundant for the annealed NCs, suggesting that their weak interaction involves hydrogen bonding to surface hydroxides. These results paint a picture of ZnO NC surfaces lightly populated with a dynamic and

complex shell of DDA ligands. This provides one explanation for the facile charge transfer reactions of these ZnO NCs,^{11,47,48} especially proton-coupled

electron transfer (PCET) reactions in which the e^-/H^+ abstractor likely has to come to the surface to remove the proton.⁹

METHODS

Chemicals. Tetramethylammonium hydroxide (TMAOH), zinc acetate dihydrate, trimethoxybenzene (TMB), and dodecylamine (DDA, 98%) were purchased from Aldrich and used as received. Toluene- d_6 and tetrahydrofuran (THF- d_6) were purchased from Cambridge Isotope, degassed by three freeze–pump–thaw cycles and (in the case of THF) dried by storage over sieves for 2 days. All other solvents were purchased from Fischer Scientific and were dried using a Seca Solvent System installed by Glass Contour. Fluka TraceCERT High Purity brand Zn standard (1000 $\mu\text{g}/\text{L}$ in 2% HCl) was used as the standard for ICP-OES which was carried out using a PerkinElmer Optima 8300. ZnO NCs were prepared by base hydrolysis from $\text{Zn}(\text{OAc})_2 \cdot 2\text{H}_2\text{O}$.²⁴ The annealed NCs were heated in molten DDA for 12 h at 160 °C.¹⁷

Microscopy and Spectroscopy. TEM images were collected using a FEI Tecnai G2 F20. Average diameter of the NCs in the batch (values in nm) were determined from the position of the first exciton peak ($d < 7 \text{ nm}$)²⁵ or from statistical analysis of TEM images using ImageJ ($d > 7 \text{ nm}$). The error is reported as 10% or as the standard deviation derived from a Gaussian fit to the histogrammed TEM, respectively. Optical spectra were acquired using a Hewlett-Packard 8453 diode array spectrophotometer.

NMR Spectroscopy. All samples were prepared under N_2 in a glovebox. 1D ^1H NMR spectra were obtained on Bruker AV300, AV301, DRX499, AV500, AV700 or AV800 (with a cryogenically cooled probehead) spectrometers, and the data were processed using MestReNova® version 7.1.2. DOSY data were collected on the DRX499, AV700, and AV800 spectrometers equipped with TBI Z gradient probe heads. The DOSY data were processed with “DOSY Toolbox” version 1.5 using Local Covariance Order Diffusion-Ordered Spectroscopy (LOCODOSY) to more effectively resolve overlapping peaks²⁸ and the results were superior to those obtained from DOSY processing with MestReNova or TopSpin. Chemical shifts are reported relative to TMS by referencing the residual solvent. ^1H NMR spectra were recorded with a 15 s delay between scans to allow full relaxation of the DDA and methyl signals of trimethoxybenzene (TMB), which was added to the NMR samples as a concentration standard. The T_1 was measured for the methyl signals of TMB and were found to be approximately 2 s. In the DOSY experiments, the pulse program used was ledppg2s, and the gradient shape SINE.100 or SMSQ10.100. The gradient duration δ and the diffusion delay Δ were optimized for each sample by comparing one slice of signals at 95% gradient strength and 5% strength (using 1D pulse program ledppg2s1d). Values were chosen which led to approximately 90% loss of the initial intensity of the peaks of interest at highest gradient, and were typically $\delta = 1\text{--}3 \text{ ms}$ and $\Delta = 100\text{--}200 \text{ ms}$. The eddy current compensation was set at 5 ms. In the full DOSY experiment, the amplitude of the sinusoidal gradient pulses was varied exponentially in strength from 5 to 95% of the maximum strength in 16 or 32 steps. Representative data are shown in Supporting Information Figure S1.

Conflict of Interest: The authors declare no competing financial interest.

Supporting Information Available: Additional NMR spectroscopy data, calculations, and figures. This material is available free of charge via the Internet at <http://pubs.acs.org>.

Acknowledgment. C.N.V. gratefully acknowledges support from the Department of Energy Office of Science Graduate Fellowship Program (DOE SCGF), made possible in part by the American Recovery and Reinvestment Act of 2009, administered by ORISE-ORAU under contract no. DE-AC05-06OR23100, and the ARCS Foundation for a fellowship. A.M.S. is funded by

the U.S. National Science Foundation Graduate Fellowship program under Grant No. DGE-1256082. We also acknowledge the Donors of the American Chemical Society Petroleum Research Fund (51178-ND3), the U.S. National Science Foundation (CHE-1151726), and the University of Washington for financial support of this research. We thank M. Braten and B. Cossairt for insightful discussions, C. E. Valdez for assistance with the illustrations, and P. Miller and R. Paranji for assistance in setting up the DOSY and NOESY NMR experiments.

REFERENCES AND NOTES

- Tian, J.; Cao, G. Semiconductor Quantum Dot-Sensitized Solar Cells. *Nano Rev.* **2013**, *4*, 22578–22585.
- Bruchez, M.; Moronne, M.; Gin, P.; Weiss, S.; Alivisatos, A. P. Semiconductor Nanocrystals as Fluorescent Biological Labels. *Science* **1998**, *281*, 2013–2016.
- Weiss, E. A. Organic Molecules as Tools To Control the Growth, Surface Structure, and Redox Activity of Colloidal Quantum Dots. *Acc. Chem. Res.* **2013**, *46*, 2607–2615.
- El-Sayed, M. A. Small Is Different: Shape-, Size-, and Composition-Dependent Properties of Some Colloidal Semiconductor Nanocrystals. *Acc. Chem. Res.* **2004**, *37*, 326–333.
- Smith, A. M.; Nie, S. Semiconductor Nanocrystals: Structure, Properties, and Band Gap Engineering. *Acc. Chem. Res.* **2009**, *43*, 190–200.
- Munro, A. M.; Jen-La Plante, I.; Ng, M. S.; Ginger, D. S. Quantitative Study of the Effects of Surface Ligand Concentration on CdSe Nanocrystal Photoluminescence. *J. Phys. Chem. C* **2007**, *111*, 6220–6227.
- Majetich, S. A.; Carter, A. C.; Belot, J.; McCullough, R. D. ^1H NMR Characterization of the CdSe Nanocrystallite Surface. *J. Phys. Chem.* **1994**, *98*, 13705–13710.
- Knowles, K. E.; Tagliazucchi, M.; Malicki, M.; Swenson, N. K.; Weiss, E. A. Electron Transfer as a Probe of the Permeability of Organic Monolayers on the Surfaces of Colloidal PbS Quantum Dots. *J. Phys. Chem. C* **2013**, *117*, 15849–15857.
- Schrauben, J. N.; Hayoun, R.; Valdez, C. N.; Braten, M.; Fridley, L.; Mayer, J. M. Titanium and Zinc Oxide Nanoparticles Are Proton-Coupled Electron Transfer Agents. *Science* **2012**, *336*, 1298–1301.
- Valdez, C. N.; Braten, M.; Soria, A.; Gamelin, D. R.; Mayer, J. M. Effect of Protons on the Redox Chemistry of Colloidal Zinc Oxide Nanocrystals. *J. Am. Chem. Soc.* **2013**, *135*, 8492–8495.
- Hayoun, R.; Whitaker, K. M.; Gamelin, D. R.; Mayer, J. M. Electron Transfer Between Colloidal ZnO Nanocrystals. *J. Am. Chem. Soc.* **2011**, *133*, 4228–4231.
- Yin, Y.; Alivisatos, A. P. Colloidal Nanocrystal Synthesis and the Organic-Inorganic Interface. *Nature* **2005**, *437*, 664–670.
- Morris-Cohen, A. J.; Malicki, M.; Peterson, M. D.; Slavin, J. W. J.; Weiss, E. A. Chemical, Structural, and Quantitative Analysis of the Ligand Shells of Colloidal Quantum Dots. *Chem. Mater.* **2012**, *1155–1165*.
- Anderson, N. C.; Hendricks, M. P.; Choi, J. J.; Owen, J. S. Ligand Exchange and the Stoichiometry of Metal Chalcogenide Nanocrystals: Spectroscopic Observation of Facile Metal-Carboxylate Displacement and Binding. *J. Am. Chem. Soc.* **2013**, *135*, 18536–18548.
- Coppel, Y.; Spataro, G.; Pagès, C.; Chaudret, B.; Maisonnat, A.; Kahn, M. L. Full Characterization of Colloidal Solutions of Long-Alkyl-Chain-Amine-Stabilized ZnO Nanoparticles by NMR Spectroscopy: Surface State, Equilibria, and Affinity. *Chem.—Eur. J.* **2012**, *18*, 5384–5393.

16. Hens, Z.; Martins, J. C. A Solution NMR Toolbox for Characterizing the Surface Chemistry of Colloidal Nanocrystals. *Chem. Mater.* **2013**, *25*, 1211–1221.

17. Norberg, N. S.; Gamelin, D. R. Influence of Surface Modification on the Luminescence of Colloidal ZnO Nanocrystals. *J. Phys. Chem. B* **2005**, *109*, 20810–20816.

18. Kalyuzhny, G.; Murray, R. W. Ligand Effects on Optical Properties of CdSe Nanocrystals. *J. Phys. Chem. B* **2005**, *109*, 7012–7021.

19. Kuno, M.; Lee, J. K.; Dabbousi, B. O.; Mikulec, F. V.; Bawendi, M. G. The Band Edge Luminescence of Surface Modified CdSe Nanocrystallites: Probing the Luminescing State. *J. Chem. Phys.* **1997**, *106*, 9869–9882.

20. Katari, J. E. B.; Colvin, V. L.; Alivisatos, A. P. X-ray Photoelectron Spectroscopy of CdSe Nanocrystals with Applications to Studies of the Nanocrystal Surface. *J. Phys. Chem.* **1994**, *98*, 4109–4117.

21. Evans, C. M.; Cass, L. C.; Knowles, K. E.; Tice, D. B.; Chang, R. P. H.; Weiss, E. A. Review of the Synthesis and Properties of Colloidal Quantum Dots: The Evolving Role of Coordinating Surface Ligands. *J. Coord. Chem.* **2012**, *65*, 2391–2414.

22. Fritzinger, B.; Moreels, I.; Lommens, P.; Koole, R.; Hens, Z.; Martins, J. C. *In Situ* Observation of Rapid Ligand Exchange in Colloidal Nanocrystal Suspensions Using Transfer NOE Nuclear Magnetic Resonance Spectroscopy. *J. Am. Chem. Soc.* **2009**, *131*, 3024–3032.

23. Canzi, G.; Mrse, A. A.; Kubiak, C. P. Diffusion-Ordered NMR Spectroscopy as a Reliable Alternative to TEM for Determining the Size of Gold Nanoparticles in Organic Solutions. *J. Phys. Chem. C* **2011**, *115*, 7972–7978.

24. Schwartz, D. A.; Norberg, N. S.; Nguyen, Q. P.; Parker, J. M.; Gamelin, D. R. Magnetic Quantum Dots: Synthesis, Spectroscopy, and Magnetism of Co^{2+} and Ni^{2+} Doped ZnO Nanocrystals. *J. Am. Chem. Soc.* **2003**, *125*, 13205–13218.

25. Meulenkamp, E. A. Synthesis and Growth of ZnO Nanoparticles. *J. Phys. Chem. B* **1998**, *102*, 5566–5572.

26. Wood, A.; Giersig, M.; Hilgendorff, M.; Vilas-Campos, A.; Liz-Marzán, L. M.; Mulvaney, P. Size Effects in ZnO: The Cluster to Quantum Dot Transition. *Aust. J. Chem.* **2003**, *56*, 1051–1057.

27. Hens, Z.; Moreels, I.; Martins, J. C. *In Situ* ^1H NMR Study on the Triethylphosphine Oxide Capping of Colloidal InP Nanocrystals. *ChemPhysChem* **2005**, *6*, 2578–2584.

28. Nilsson, M. The DOSY Toolbox: A New Tool for Processing PFG NMR Diffusion Data. *J. Magn. Reson.* **2009**, *200*, 296–302.

29. Sandström, J. *Dynamic NMR Spectroscopy*; Academic Press Inc.: New York, 1982.

30. Chen, J.; Ruther, R. E.; Tan, Y.; Bishop, L. M.; Hamers, R. J. Molecular Adsorption on $\text{ZnO}(1010)$ Single-Crystal Surfaces: Morphology and Charge Transfer. *Langmuir* **2012**, *28*, 10437–10445.

31. Hanada, T. Basic Properties of ZnO, GaN, and Related Materials. In *Oxide and Nitride Semiconductors*; Yao, T., Hong, S.-K., Eds.; Springer: Berlin Heidelberg, 2009; Vol. 12.

32. Hinterwirth, H.; Kappel, S.; Waitz, T.; Prohaska, T.; Lindner, W.; Lämmerhofer, M. Quantifying Thiol Ligand Density of Self-Assembled Monolayers on Gold Nanoparticles by Inductively Coupled Plasma–Mass Spectrometry. *ACS Nano* **2013**, *7*, 1129–1136.

33. Anderson, N. C.; Owen, J. S. Soluble, Chloride-Terminated CdSe Nanocrystals: Ligand Exchange Monitored by ^1H and ^{31}P NMR Spectroscopy. *Chem. Mater.* **2012**, *25*, 69–76.

34. Moreels, I.; Martins, J. C.; Hens, Z. Ligand Adsorption/Desorption on Sterically Stabilized InP Colloidal Nanocrystals: Observation and Thermodynamic Analysis. *ChemPhysChem* **2006**, *7*, 1028–1031.

35. Hassinen, A.; Gomes, R.; De Nolf, K.; Zhao, Q.; Vantomme, A.; Martins, J. C.; Hens, Z. Surface Chemistry of CdTe Quantum Dots Synthesized in Mixtures of Phosphonic Acids and Amines: Formation of a Mixed Ligand Shell. *J. Phys. Chem. C* **2013**, *117*, 13936–13943.

36. Hassinen, A.; Moreels, I.; De Nolf, K.; Smet, P. F.; Martins, J. C.; Hens, Z. Short-Chain Alcohols Strip X-Type Ligands and Quench the Luminescence of PbSe and CdSe Quantum Dots, Acetonitrile Does Not. *J. Am. Chem. Soc.* **2012**, *134*, 20705–20712.

37. Gomes, R.; Hassinen, A.; Szczygiel, A.; Zhao, Q.; Vantomme, A.; Martins, J. C.; Hens, Z. Binding of Phosphonic Acids to CdSe Quantum Dots: A Solution NMR Study. *J. Phys. Chem. Lett.* **2011**, *2*, 145–152.

38. De Roo, J.; Van den Broeck, F.; De Keukeleere, K.; Martins, J. C.; Van Driessche, I.; Hens, Z. Unravelling the Surface Chemistry of Metal Oxide Nanocrystals, the Role of Acids and Bases. *J. Am. Chem. Soc.* **2014**, *136*, 9650–9657.

39. Madelung, O. *Semiconductors: Data Handbook*, 3rd ed.; Springer: New York, 2004.

40. Bullen, C.; Mulvaney, P. The Effects of Chemisorption on the Luminescence of CdSe Quantum Dots. *Langmuir* **2006**, *22*, 3007–3013.

41. Song, B.; Reuber, J.; Ochs, C.; Hahn, F. E.; Lügger, T.; Orvig, C. Effects of Sequential Replacement of $-\text{NH}_2$ by $-\text{OH}$ in the Tripodal Tetraamine Tren on Its Acidity and Metal Ion Coordinating Properties. *Inorg. Chem.* **2001**, *40*, 1527–1535.

42. Vohs, J. M. Site Requirements for the Adsorption and Reaction of Oxygenates on Metal Oxide Surfaces. *Chem. Rev.* **2012**, *113*, 4136–4163.

43. Jagadish, C.; Pearton, S. J. *Zinc Oxide Bulk, Thin Films and Nanostructures*; Elsevier Ltd.: Amsterdam, 2006.

44. Henrich, V. E.; Cox, P. A. *The Surface Science of Metal Oxides*; Press Syndicate of the University of Cambridge: Cambridge, 1994.

45. Wilkinson, G.; Gillard, R. D.; McCleverty, J. A. *Comprehensive Coordination Chemistry*; Pergamon Books Ltd.: Oxford, Great Britain, 1987; Vol. 5.

46. McCleverty, J. A.; Meyer, T. J. *Comprehensive Coordination Chemistry II*; Elsevier Ltd.: Oxford, U.K., 2004; Vol. 6.

47. Morris-Cohen, A. J.; Frederick, M. T.; Cass, L. C.; Weiss, E. A. Simultaneous Determination of the Adsorption Constant and the Photoinduced Electron Transfer Rate for a CdS Quantum Dot–Viologen Complex. *J. Am. Chem. Soc.* **2011**, *133*, 10146–10154.

48. Morris-Cohen, A. J.; Aruda, K. O.; Rasmussen, A. M.; Canzi, G.; Seideman, T.; Kubiak, C. P.; Weiss, E. A. Controlling the Rate of Electron Transfer between a Quantum Dot and a Tri-Ruthenium Molecular Cluster by Tuning the Chemistry of the Interface. *Phys. Chem. Chem. Phys.* **2012**, *14*, 13794–13801.